ORIGINAL PAPER

CrossMark

An Investigation on Magnetic-Interacting Fe_3O_4 Nanoparticles Prepared by Electrochemical Synthesis Method

N. Rezaei[1] · M. H. Ehsani[1] · Mustafa Aghazadeh[2] · Isa Karimzadeh[3]

Abstract

Naked, polyvinylchloride (PVC)-coated, and polyethylene glycol (PEG)-coated Fe_3O_4 nanoparticles (NPs) with an equivalent average particle size of 10 nm were prepared through an electrochemical synthesis method. The structural and magnetic properties were investigated systematically. The X-ray diffraction study coupled with the Rietveld refinement of XRD data showed that samples are crystallized in cubic spinel structure with space group referred to as Fd3m. The nature of DC magnetization versus field M (H) plot for sample resembles qualitatively with ferromagnetic (FM) systems. The AC-susceptibility data obtained at different frequencies confirmed the presence of a frequency-dependent freezing temperature. Based on the interparticle interaction strength and phenomenological models (Néel–Brown, Vogel–Fulcher, and critical slowing down), the magnetic dynamic behavior of nanoparticles was characterized. By fitting the experimental data with mentioned models, the possibility existence of superparamagnetic and a spin-glass state at low temperatures was proposed for the samples. Also, the obtained values from fitting performance showed a coating effect on interparticle interaction for PVC- and PEG-coated Fe_3O_4 nanoparticles.

Keywords Ferromagnetic · Magnetic interacting · Nanoparticles · AC susceptibility

1 Introduction

Magnetic materials have attracted considerable scientific interest due to their use in physical properties such as magnetic recording media, magnetic sensors, permanent magnets, magnetic resonance imaging enhancement, ferrofluids, magnetic refrigeration, and magnetically guided drug delivery. Among these materials, nanoparticles (NPs) have richer electronic and magnetic properties arising from the structural and magnetic disorder in the grain surfaces. Their properties intensively depend on size, shape, particle size distribution, and interactions between nanoparticles [1–3]. In fact, when the size of a particle becomes smaller to single domain size, each particle has a large magnetic moment (the so-called superspin) [3]. In this case, the interaction strength can play a critical factor. Noninteracting superspins lead to a superparamagnetic (SPM) behavior. In the SPM regime, each particle behaves like a paramagnetic atom and the magnetic nanoparticles experience a SPM relaxation process, in which instead of fixing the magnetization along certain direction, it rapidly fluctuates. Above a certain temperature known as the blocking temperature (T_B), the magnetic anisotropy energy of a nanoparticle is overcome by the thermal activation. If the interactions between the superspins, which are fully frustrated and random, and become sufficiently strong, the system goes through the superspin-glass state at below a freezing temperature [3]. It is mentionable that the magnetic interactions in fine particle can be classified as (i) dipole–dipole interactions, which always exist, (ii) exchange interactions through the surface of the particles which are in close contact, and (iii) in

✉ M. H. Ehsani
  Ehsani@semnan.ac.ir

1 Department of Physics, Semnan University, P.O. Box 35195-363, Semnan, Iran

2 Materials and Nuclear Research School, Nuclear Science and Technology Research Institute (NSTRI), P.O. Box 14395-834, Tehran, Iran

3 Department of Physics, Faculty of Science, Central Tehran Branch, Islamic Azad University, Tehran, Iran

granular solids, Ruderman–Kitel–Kasuya–Yosida (RKKY) interactions through a metallic matrix when particles are also metallic and superexchange interactions when the matrix is insulating [3].

Vargas et al. indicated that by increasing interparticle interactions, the blocking temperature of a system of Fe_3O_4 nanoparticles increases, but H_c decreases. They said that demagnetization role of dipole–dipole interactions reduces the H_c of the system [4]. Nadeem et al. demonstrated an enhance H_c and blocking temperature of compacted Fe_3O_4 nanoparticles compared with the powder samples. They justified this result by highlighting the effect of interparticle interactions on the energy barrier between equilibrium states [5]. Hansen and Morup indicated that for weakly interacting nanoparticles, the energy barrier decreases with increasing the interactions [6].

Up now, various chemical-based preparation routes including co-precipitation, sol-gel, solvothermal, hydrothermal, and thermal decomposition methods have been developed for the fabrication of magnetite nanoparticles (MNPs) with proper magnetic and physico-chemical properties. In addition to these methods, electrochemical-based routes, i.e., cathodic electrosynthesis (CE) can be applied for facile preparation of MNPs, which have advantages of facility and ability of controlling the purity, crystallinity, and size of electro-synthesized NPs by manipulating the applied electrochemical conditions [7]. In this regard, it was reported that fine nanoparticles of metal oxides/hydroxides including $Co(OH)_2$, $Ni(OH)_2$, $Y(OH)_3$, $Zr(OH)_2$, ZrO_2, Y_2O_3, Mn_3O_4, and NiO could be easily fabricated through a one-pot CE procedure [8–13]. However, this method has been rarely applied for the preparation of MNPs until now.

In this work, we report Fe_3O_4 nanoparticles coated with polyethylene glycol (PEG) and polyvinylchloride (PVC) polymers prepared through a facile CE procedure and investigation of their interparticle interactions. To the best of our knowledge, there is no report about investigation of magnetic interactions of Fe_3O_4 nanoparticles coated with PEG and PVC. In this paper, the effect of magnetostatic interaction strength and pressure on spin dynamics, magnetization, and anisotropy of samples has been investigated using AC and DC magnetic measurements.

2 Materials and Methods

Ferrous chloride tetrahydrate ($FeCl_2 \bullet 4H_2O$, 99%), ferric nitrate nonahydrate ($Fe(NO_3)_3 \bullet 9H_2O$, 99.9%), PVC, and PEG ($M_w = 4000$) were purchased from Sigma-Aldrich. All materials were used without any further purification.

The CE platform previously reported for the fabrication of naked and coated MNPs [14–17], was here modified for the electrosynthesis of iron oxide nanoparticles from ethanol medium. The electrosynthesis set-up was composed of a (316 L, 5 cm × 5 cm × 0.5 mm) steel cathode centered between two parallel graphite anodes. The deposition bath includes 2.4 g iron(III) nitrate- and 1.2 g iron(II) chloride-dissolved 96% ethanol–4% water solution. The electrodeposition runs were conducted on an electrochemical workstation system (Potentiostat/Galvanostat, Model NCF-PGS 2012, Iran) with applying a DC current density of 10 mA cm^{-2}. For preparation of PEG- and PVC-coated NPs, composition of electrolyte was just changed and PEG or PVC polymers (1 g L^{-1}) were added to the deposition bath. After each deposition run, the cathode was brought out from the deposition bath and rinsed several times with deionized H_2O. Then, the deposited black films were scraped from the steel and subjected to separation and purification steps, which include the following; (i) the obtained wet powders were dispersed in deionized water and centrifuged at 6000 rpm for 20 min to remove free anions and weakly bounded and/or uncoated polymers, (ii) the deposit was then separated from water solution by a magnet, dried in a vacuum oven, and (iii) the resulting black dry powders were named F, F_{PEG}, and F_{PVC} for naked, PEG-coated, and PVC-coated iron oxides, respectively, and used for further evaluations.

A transmission electron microscopy (TEM, Phillips EM 208 with an accelerating voltage of 80 kV) was used to determine the size and morphology of the prepared NPs. The X-ray diffraction (XRD) patterns of the prepared NPs were obtained by XRD of powder (Phillips Model X'PERT MPD with Co Kα radiation ($\lambda = 1.789$ Å). Magnetization versus field measurements at room temperature were performed using a quantum design SQUID magnetometer, equipped with a superconducting coil which produces magnetic fields in the range from -20 to $+20$ kOe. Zero-field cooling (ZFC) and field cooling (FC) magnetizations were measured in a static magnetic field of 10 Oe. AC magnetic susceptibility measurements were performed in a quantum design physical property measurement system (PPMS). The measurements were carried out by cooling the samples from room temperature to 5 K in zero magnetic field, then the susceptibility were measured in a warming process in a magnetic field of 10 Oe and frequencies of 100 Hz to 10 kHz.

3 Results and Discussion

Figure 1 shows XRD patterns of the electro-synthesized F, F_{PEG}, and F_{PVC} nanoparticles. The XRD results of F, F_{PEG}, and F_{PVC} samples revealed the existence of a crystalline spinal structure (JCPDS 01-088-0315). The presence of plates (111), (220), (311), (400), (422), (511) and (440) on the angles of the order 7437 675 6308 5068 4150 3506, and
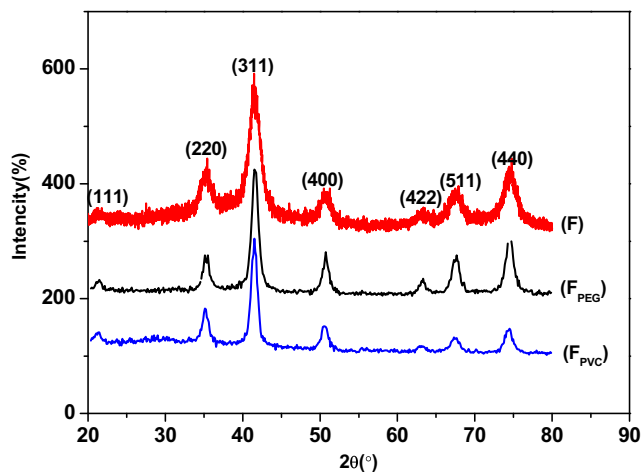
Fig. 1 XRD patterns of the F, F_{PEG}, and F_{PVC} nanoparticles

21.35, respectively, diffraction pattern of nanoparticles in the formation of a cubic spinel structure with space group referred to as Fd3m. The maximum intensity at an angle of 4150 relating to (311) is observed. The crystallite size D and lattice constant (a) were also calculated using Scherrer's equation and diffraction patterns of XRD analysis.

$$D = \frac{K\lambda}{\beta \cos\theta} \tag{1}$$

where β is the full width at half maximum (FWHM) of the XRD peaks, θ is the Bragg angle, K (~ 0.9) is the Scherrer's constant and related to the shape of crystallites and λ is wave length of the X-ray [18]. The structure parameters of F, F_{PEG}, and F_{PVC} samples are provided in Table 1.

Coated iron oxide nanoparticles, without a significant structural change can improve its resistance to acids and prevent phase changes of this compound. According to Table 1, F_{PEG} and F_{PVC} samples have a smaller crystallite size and the maximum size corresponds to the sample F One of the effects of reducing the crystallite size changes the lattice constants of the material and increases the pressure and stress on the particle surface. Kumar et al. by incrementing the Al content observed a decrease in crystallite size, which attributed the decrease in crystallite size to the increase of stress inside the sample [19] As shown in Table 1 the lattice constant F sample is a large amount compared with the

F_{PEG} and F_{PVC} samples. This can be related to the fact that with grain size reduction, the surface effects became dominant. One of these effects is the hydrostatic pressure on the grain which led to the modification on the volume of cells and the lattice constant Indeed, the lattice constant of the nanostructured ferrite changes creating internal stresses in the structure of the samples. As observed reducing the particle size reduced the lattice parameters which can change the distribution of spinel structure in cations [20–24].

Figure 2 shows TEM micrographs of F, F_{PEG}, and F_{PVC} samples. The size dispersion histogram was determined using the method described by Lavorato et al. [22] The size dispersion was fitted with a log-normal function $f(D) = (1/\sqrt{2\pi}\sigma D)\exp[Ln^2(D/D)/2\sigma^2]$ and then the median diameter D and dispersion σ were determined Using the fit results, the mean diameter $D = D_0 \exp(\sigma^2/2)$ and standard deviation standard deviation $\sigma_D = \langle D \rangle (\exp(\sigma^2) - 1)^{\frac{1}{2}}$ were calculated. The mean diameter TEM of particles and the standard deviation are shown in Table 1. The difference between D_{TEM} and D_{XRD} suggests the formation of a coating layer and an amorphous (dead) layer at the surface of NPs. The thickness of magnetic dead layer has sometimes been estimated using magnetic hysteresis loop measurements.

The magnetic properties of the prepared naked and PEG-coated NPs were determined using Lake Shore Model 7410 vibrational sample magnetometer (VSM) from -20 to 20 KOe at room temperature. Also, the magnetic hysteresis and saturation magnetizations of naked PEG-coated, and PVC-coated NPs were evaluated and shown in Fig. 3 Saturation magnetization value (M_s), coercivity field (H_c), and magnetic hysteresis of F, F_{PEG}, and F_{PVC} samples were calculated and presented in Table 2. Small coercivity (H_C) of the samples shows the superparamagnetic behavior, and H_C enhancement observed in F_{PEG} and F_{PVC} samples show the single-domain property of the NPs. The saturation magnetization decreases with coating the NPs. This slight reduction can be attributed to magnetic core size reduction and the surface effects on magnetization value. In order to estimate the surface spin contribution to total magnetization, the hysteresis loops were fitted with the modified Langevin function [25]:

$$M = M_s L\left(\frac{\mu_p H}{k_B T}\right) + \chi H \tag{2}$$

Table 1 Structure parameters of F, F_{PEG}, and F_{PVC} samples

Sample	2θ (deg)	FWHM (2θ) (311)	a (Å)	D_{XRD} (nm)	D_{TEM} (nm)	σ_D (nm)
F	41.50	1.26	8.3734	7.79	8.22	1.54
F_{PEG}	41.56	1.76	8.3612	5.64	7.82	1.14
F_{PVC}	41.45	1.73	8.3651	5.74	9.33	1.9

Fig. 2 TEM micrograph of F, F_{PEG}, and F_{PVC} samples
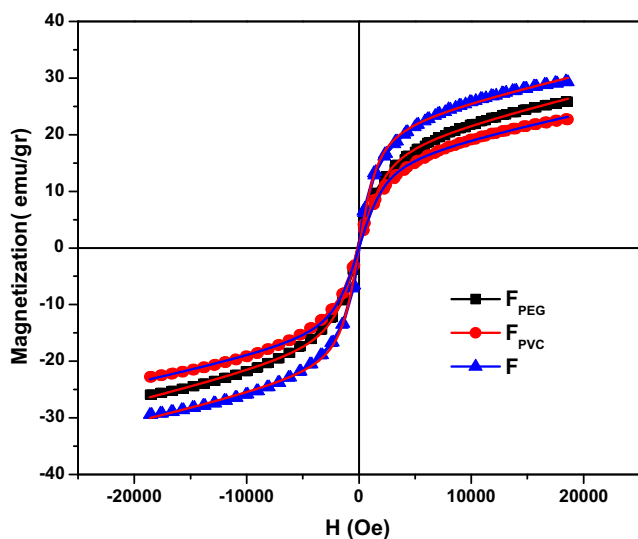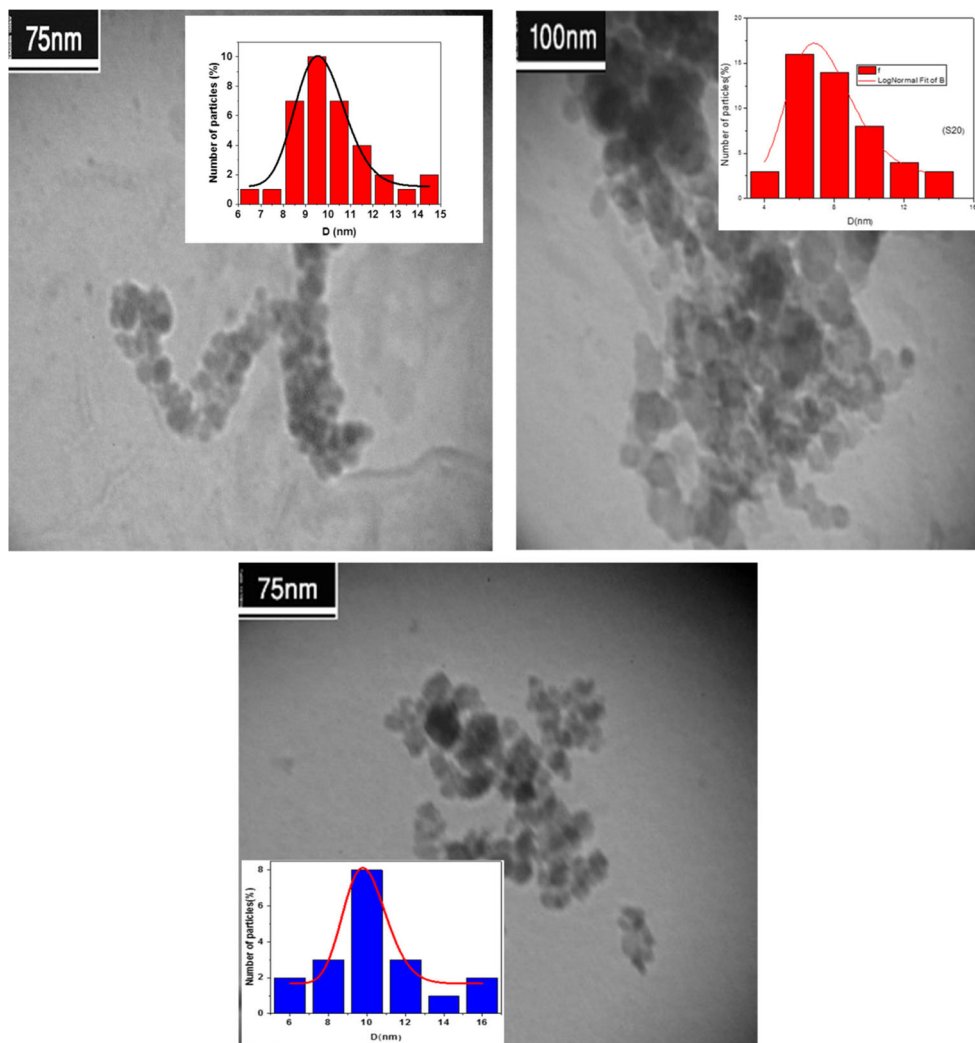
Fig. 3 The hysteresis loops (M–H curves) of F, F_{PEG}, and F_{PVC} samples at room temperature

Here T is temperature, H is applied magnetic field, K_{B} is the Boltzmann constant, μ_p is the average moment, L is the Langevin function and χ is the high field susceptibility that arises from the paramagnetic surface spin contribution [26]. The calculated values with fitting for $M_s \chi$, and μ_p are reported in Table 2. The μ_p and M_s values are found to decrease in coated NPs as a consequence of particle size reduction. Also, the χ change suggests the

Table 2 Magnetic parameter: calculating and fitting of the F, F_{PEG}, and F_{PVC} samples

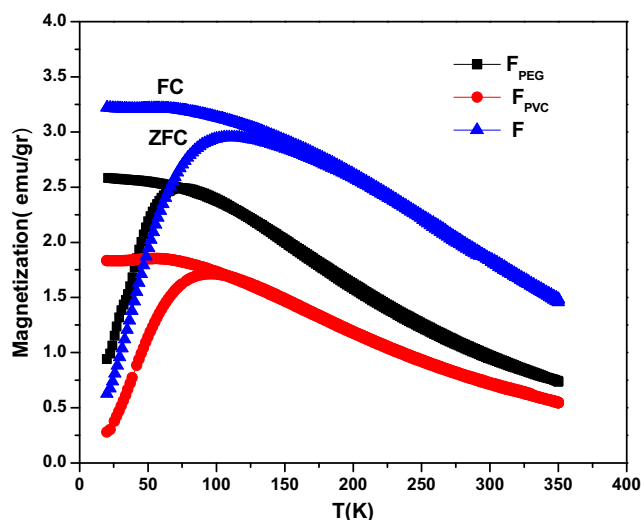| Parameter	F	F_{PEG}	F_{PVC}
H_{c} (Oe)	8.7	12.8	13.4
M_{r} (emu/g)	104.1×10^{-3}	67.4×10^{-3}	21.7×10^{-3}
μ_{P} (μ_{B})	14553	10300	10301
M_{s} (emu/g)	22.33	16.26	18.49
χ (emu/gO$_{\text{c}}$)	4.5×10^{-4}	4.1×10^{-4}	4.7×10^{-4}
t (nm)	0.98	0.77	0.76

Fig. 4 ZFC and FC curves of the Fe_3O_4 samples

surface contribution to total magnetization. To calculate the thickness of dead layer, the following function was used [27]:

$$M_s = M_B(1 - \frac{6t}{d}) \qquad (3)$$

Here t is the deadlayer thickness d is the diameter of particles and M_B is the bulk saturation magnetization. The values of the dead-layer thickness are reported in Table 2. Results show that the dead-layer thickness was decrease with a decrease in NPs. Magnetization is made up of the two magnetic core and the shell ($M_{tot} = M_{core} + M_{shell}$) in which the magnetization of the shell is almost zero (M_{shell}). This means that by reducing the particle size the nuclear magnetization is increased.

In order to study the coated effects on Fe_3O_4 nanoparticles and size effects on magnetic properties, the temperature dependence of the magnetization $M(T)$ was measured. In the $M(T)$ curves we always obtained two different curves for ZFC and FC programs for superparamagnetic materials. In the ZFC curve, the moment increased with the temperature and then decreased, while the moment decreased in the FC curve. The temperature at the peak point of the ZFC curve is the blocking temperature. The Néel relaxation time mentioned above is strongly temperature dependent as generally the fluctuation of magnetizations is larger at higher temperature and smaller at lower temperature [28]. At the single-domain structure, superparamagnetic materials can fluctuate randomly by thermal fluctuation at high enough temperatures just as an atom spin in paramagnetic materials. At low temperatures, the thermal energy becomes smaller and the magnetic moments become blocked. This temperature is the blocking temperature. Below the blocking temperature, superparamagnetic material loses its preferred direction of magnetization in zero magnetic fields [29].

Temperature dependence of magnetization $M(T)$ behavior for the F, F_{PVC}, and F_{PEG} samples was calculated in the ZFC and FC modes at an applied magnetic field of 10 Oe. Figure 4 shows the FC and ZFC magnetizations of the F, F_{PVC}, and F_{PEG} samples in the field of 10 Oe. For the F, F_{PVC}, and F_{PEG} samples, with increases of temperature the ZFC curves increase to a maximum at $T_{max} = \beta \langle T_B \rangle$. Here $\langle T_B \rangle$ is the average blocking temperature and β is the constant ($\beta = 1$–2.5) which depends on the T_B distribution [30]. From Fig. 4, it can be seen the decreasing of magnetization in ZFC mode below T_B which is similar superparamagnetic behavior [31]. The increase of the magnetic anisotropy of the F, F_{PVC}, and F_{PEG} samples is a probable reason for the indicated decrease of the FC and ZFC magnetizations with compaction and interactions between NPs. With coated Fe_3O_4 nanoparticles using PEG and PVC, the T_B decreases. The values of T_B for the F, F_{PVC}, and F_{PEG} samples obtained were 115, 75 and 59 K, respectively.

Theoretical blocking temperature can be calculated from the below function:

$$T_B = \frac{kV}{25k_B} \qquad (4)$$

where $K_B = 1 / 38 \times 10^{-16}$ erg deg^{-1} is the Boltzmann constant k is the magnetic anisotropy constant which is 1.4×10^4 erg cm^{-3}, and $V = \frac{4}{3}\pi R^3$ is the average volume of nanoparticles; here R was calculated by TEM results [32]. The values of V obtained for the F, F_{PVC}, and F_{PEG} samples were 2.9×10^{-17}, 5.1×10^{-17}, and 2.5×10^{-17} cm^3, respectively. The values of the theoretical T_B obtained for the F, F_{PVC}, and F_{PEG} samples were 11.8, 20.8 and 10.2, respectively. This result indicated that the interaction between nanoparticles shows that the interaction between nanoparticles can affect the blocking/freezing temperature by modifying the potential barrier [33].

In order to obtain the type of interaction between nanoparticles, the dynamic behavior of the samples were studied by AC-susceptibility measurements in an AC field of 10 Oe at a frequency of 100, 1000, 2000, 5000, and 10000 Hz as a function of temperature. The real part (χ'), and imaginary part (χ''), of the AC susceptibility of the samples as a function of temperature is shown in Fig. 5.

Similar plots were determined for the other samples too. As one can see, T_p shifts toward higher temperatures by increasing frequencies. Frequency dependence of T_p is a description of a superparamagnetic and glass system [34, 35]. Noninteraction nanoparticle relation between T_P and relaxation time is given by the τ_0 Néel–Brown model [36]:

$$\tau = \tau_0 \exp\left(\frac{E_a}{K_B T_B}\right) \qquad (5)$$

where $E_a = KV$ is energy barrier, which K is the magnetic anisotropy constant and V is the volume of particles;
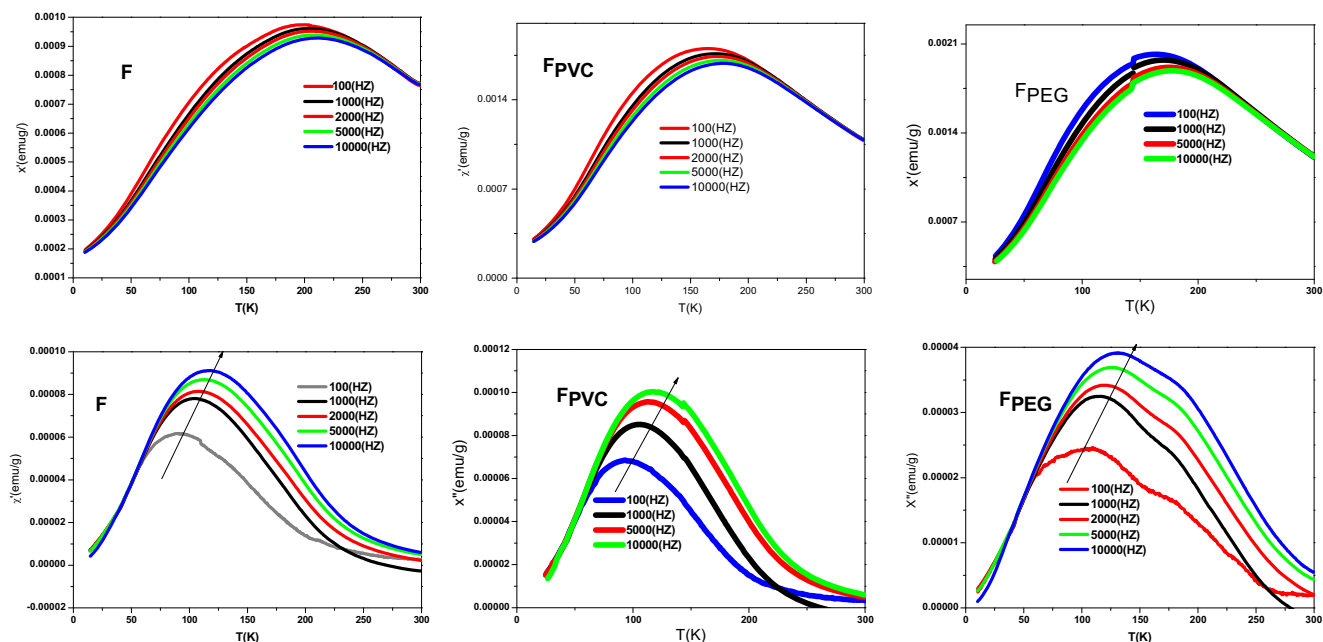
Fig. 5 The real part χ', and imaginary part χ'', of AC susceptibility of the samples as a function of temperature

τ_0 for a spin system is about 10^{-9}–10^{-13} s [37], $\tau = 1/2\pi f$ is related to measurement frequency and K_B is Boltzmann constant. Figure 6 shows the results of fitting the experimental data by (5). Our estimated values of τ_0 and E_a for the F, F_{PVC}, and F_{PEG} samples are given in Table 3. In the Néel–Brown model, for the noninteraction particles the value of τ_0 is about 10^{-9}–10^{-13} s, but as can be seen the values of τ_0 are too small. This result showed that the samples are interacting between particles. For assemblies

of weakly interacting magnetic nanoparticles, the frequency dependence of T_P is given by using the Vogel–Fulcher law [38, 39]:

$$\tau = \tau_0 \exp\left(\frac{E_a}{K(T_P - T_0)}\right) \tag{6}$$

In fact, (6) is another form of the Néel–Brown law. In (6), T is an effective temperature and a factor of interaction strength confirmed that the compaction of particles influenced the dipole–dipole interactions. Kura et al. [40] indicated that there is a strong dipole–dipole interaction in agglomerate $\alpha - Fe$ particles and energy barrier by Vogel–Fulcher model could not be estimated form the Néel–Brown model. In Fig. 7 we tried to best fit the experimental data on the real part of the F, F_{PVC}, and F_{PEG} samples with (6). The estimated fitting are given in Table 3. In the coated samples, obtained results decrease in T with increasing the grinding time indicating that the interparticle interaction energy decreased. At low temperatures, interactions cause the formation of a frustrated frizzed state of superspin called spin glass. To classify the observed blocking/freezing process and to study the dynamics of spins and determin the kind of interactions [41, 42], useful parameters C_1 and C_2 are usually used [43]:
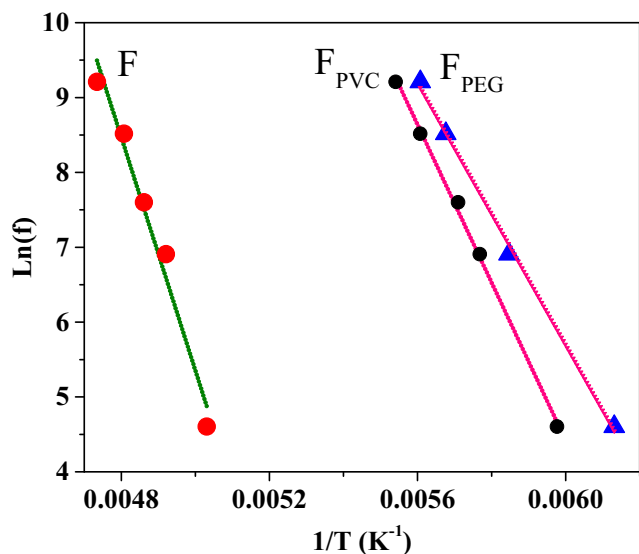

Fig. 6 Results of fitting of AC magnetic susceptibility data using the Néel–Brown model

$$C_1 = \frac{\Delta T_p}{T_p \Delta(\log f)} \tag{7}$$

$$C_2 = \frac{T_p - T_0}{T_P} \tag{8}$$

Table 3 The fitting parameters using the Néel–Brown, Vogel–Fulcher, and critical slowing down models

Model	Parameter	F	F_{PVC}	F_{PEG}
Néel–Brown	$\tau_0(s)$	2.1×10^{-29} s	0.41×10^{-29}	5.19×10^{-26}
	$E_a/K_B(K)$	11,978.78	10,557.35	8757.005
Vogel–Fulcher	$\tau_0(s)$	3.67×10^{-11}	1.25×10^{-12}	7.23×10^{-11}
	$E_a/K_B(K)$	1013.91	1194.024	1479.36
	$T_0(K)$	143	115	100
Critical slowing down	$\tau_0(s)$	2.702×10^{-10}	6.93×10^{-7}	2.003×10^{-9}
	Zv	8.69	10.61	10.52
	$T_0(K)$	172	143	135

where ΔT_p is the difference between T_P measured at the frequency $\Delta(\log f)$ interval and T_P is the mean value of blocking/freezing temperature. The values of C_1 and C_2 depend on the interaction strength between nanoparticles and decreases by increasing the interactions between particles. Based on the calculated values of C, there are three types: noninteracting nanoparticles ($C > 0.13$), medium interaction ($0.05 < C < 0.13$), and for spin glasses ($0.005 < C < 0.05$) [43, 44]. In Table 3 estimated values of C_1 and C_2 are given for the F, F_{PVC}, and F_{PEG} samples. Our calculated values for C_1 were about 0.02 for all samples, which is in the range of those reported for spin glasses [41]. We find $C_2 \approx 0.12$ which is also close to the spin-glass systems [43]. The values of C_1 and C_2 decrease by increasing the nanoparticle size. With the increase of the nanoparticle size magnetic moment and dipole–dipole interaction increase and C_1 and C_2 values decrease. The possibility of existence of spin glass behavior can be checked by critical slowing down model [45]. In this model relaxation time, τ is expressed by the following equation [46]:

$$\tau = \tau_0 \left(\frac{T_P}{T_0 - 1} \right)^{-Zv} \tag{9}$$

In this equation τ_0 is related to the relaxation time of the individual particle magnetic moment; Zv as a dynamic critical exponent shows interactions strength and values between 4 and 12 for spin glasses, reentrant spin glasses and superspin glasses [47]. From best fits of this model we calculated Zv values for the F, F_{PVC}, and F_{PEG} samples. The values of the F, F_{PVC}, and F_{PEG} samples are reported in Table 3. Relaxation time change shows that the frustration and collective freezing of superspins became weaker by coating.

Given the frequency dependence of the magnetic response of samples, we were interested in studying their power loss. Within the validity of linear response theory the loss power density P is related to χ'' according to the succeeding equation

$$P = \mu_0 \pi \chi'' f H^2 \tag{10}$$

where μ is vacuum permeability, f is applied frequency, and H is external magnetic field [48] The value of P can be under the influence of different parameters like applied field and frequency, magnetic interactions size distribution, anisotropy, etc In order to investigate the effect of magnetic interactions on loss power density, the P values have been estimated using (10). The values of P versus temperature were calculated for the F, F_{PVC}, and F_{PEG} samples at various frequencies of 10, 100, 1000 and 10,000 as presented in the plots in Fig. 8. The minimum value of P belongs to the sample F. By coating the F sample using F_{PVC} and F_{PEG} values of P increased Clearly, the maximum value of P belongs to the F_{PEG} sample, which shows the increase in the magnetic interactions between nanoparticles.
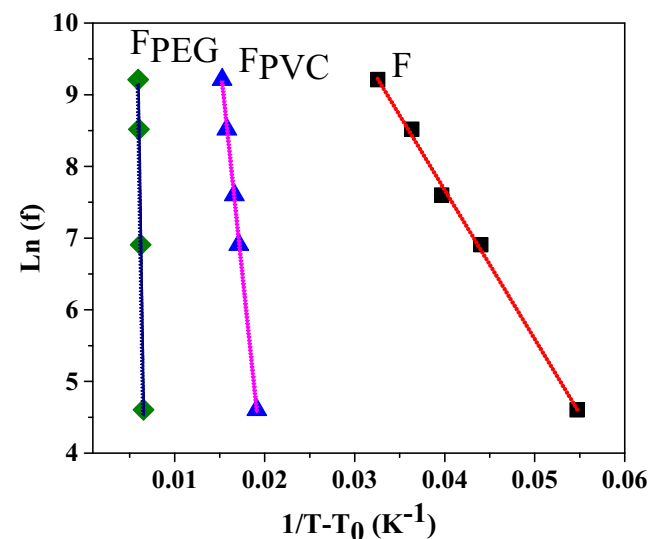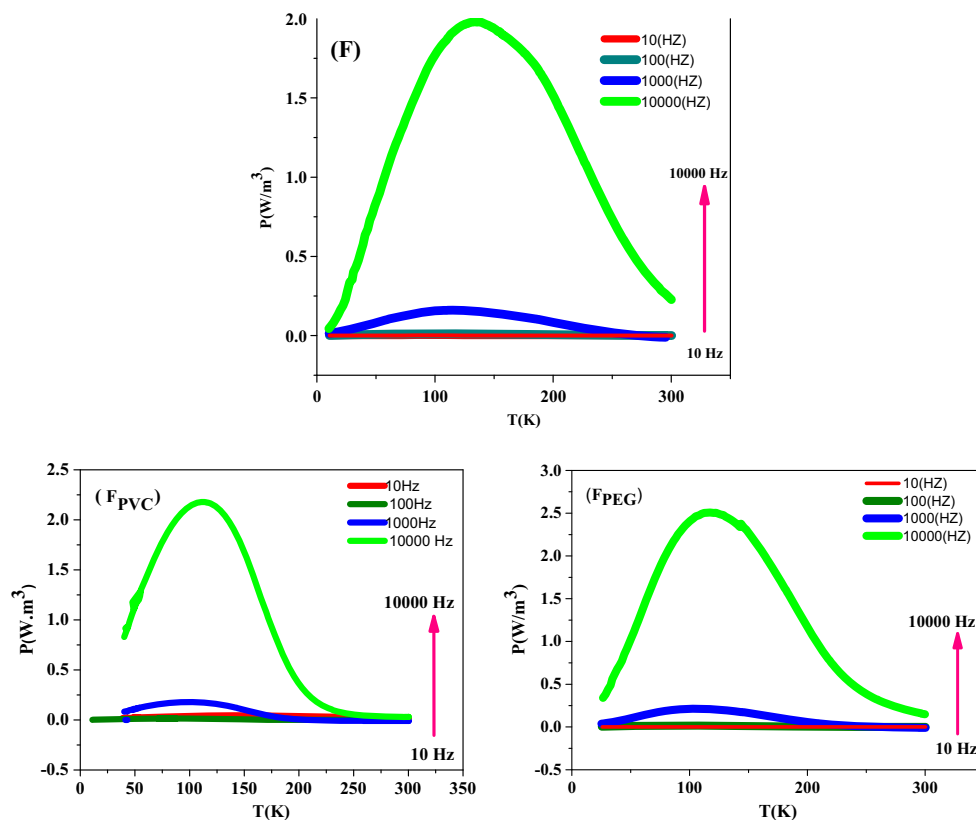

Fig. 7 Results of fitting of AC magnetic susceptibility data using the Vogel–Fulcher model

Fig. 8 Loss power density of the F, F_{PVC}, and F_{PEG} samples versus temperature

4 Conclusion

In this paper, Fe_3O_4 nanoparticles coated with PEG and PVC nanoparticles were prepared by facile cathodic electrodeposition method. The effect of dipole–dipole interactions and powder compaction on magnetic properties has been investigated through dynamic magnetic measurements. By increasing the compaction of powders, the interparticle interactions strength increased. From different AC and DC magnetic characterizations, it was understood that magnetostatic interactions increase the magnetic hardness including H_c, H_a, and effective anisotropy constant (K_{eff}) of the samples. Increase of H_c by increasing the applied pressure confirms the presence of interacting unblocked nanoparticles in the samples. The observed decease in the FC and ZFC magnetizations by increasing the powder compaction was attributed to the presence of random dipole–dipole interactions.

References

1. Mendonça, E.C., Jesus, C.B.R., Folly, W.S.D., Meneses, C.T., Duque, J.G.S.: Size effects on the magnetic properties of ZnFe$_2$O$_4$ nanoparticles. J. Supercond. Nov. Magn **26**, 2329–2331 (2013)

2. Nagahama, T., Matsuda, Y., Tate, K., Kawai, T., Takahashi, N., Hiratani, S., Watanabe, Y., Yanase, T., Shimada, T.: Magnetic properties of epitaxial Fe3O4 films with various crystal orientations and tunnel magnetoresistance effect at room temperature. Appl. Phys. Lett. **105**, 102410 (2014)

3. Guimarães, A.P. Principles of Nanomagnetism, 1st Edn. Springer-Verlag, Berlin (2009)

4. Vargas, J.M., Nunes, W.C., Socolovsky, L.M., Knobel, M., Zanchet, D.: Effect of dipolar interaction observed in iron-based nanoparticle. Phys. Rev. B **72**(18), 184428–184434 (2005)

5. Nadeem, K., Krenn, H., Traussnig, T., Wurschum, R., Szabó, D., Letofsky-Papst, I.: Effect of dipolar and exchange interactions on magnetic blocking of maghemite nanoparticles. J. Magn. Magn. Mater. **323**, 1998–2004 (2011)

6. Hansen, M.F., Mørup, S.: Models for the dynamics of interacting magnetic nanoparticles. J. Magn. Magn. Mater. **184**, 262–274 (1998)

7. Aghazadeh, M., Hosseinifard, M.: Electrochemical preparation of ZrO$_2$ nanopowder: impact of the pulse current on the crystal structure, composition and morphology. Ceram. Int. **39**, 4427–4435 (2013)

8. Aghazadeh, M., Yousefi, T., Ghaemi, M.: Low-temperature electrochemical synthesis and characterization of ultrafine Y(OH)$_3$ and Y$_2$O$_3$ nanoparticles. J. Rare Earths **30**, 236–240 (2012)

9. Aghazadeh, M., Maragheh, M.G., Ganjali, M.R., Norouzi, P.: Preparation and characterization of Mn$_5$O$_8$ nanoparticles: a novel and facile pulse cathodic electrodeposition followed by heat-treatment. Inorganic and Nano-Metal Chemistry **27**, 1085–1089 (2017)

10. Aghazadeh, M., Barmi, A.A.M., Hosseinifard, M.: Nanoparticulates Zr(OH)$_4$ and ZrO$_2$ prepared by low-temperature cathodic electrodeposition. Mater. Lett. **73**, 28–31 (2012)

11. Aghazadeh, M., Malek Barmi, A.A., Gharailou, D., Peyrovi, M.H., Sabour, B., Najafi, F.: Cobalt hydroxide ultra-fine nanoparticles with excellent energy storage ability. Appl. Surf. Sci. **283**, 871–875 (2013)

12. Aghazadeh, M., Nozad Golikand, A., Ghaemi, M.: Synthesis, characterization, and electrochemical properties of ultrafine β-Ni(OH)$_2$ nanoparticles. Int. J. Hydrogen Energy **36**, 8674–8679 (2011)

13. Barani, A., Aghazadeh, M., Ganjali, M.R., Sabour, B., Barmi, A.A.M., Dalvand, S.: Nanostructured nickel oxide ultrafine nanoparticles: synthesis, characterization, and supercapacitive behavior. Mater. Sci. Semicond. Process. **23**, 85–92 (2014)

14. Karimzadeh, I., Aghazadeh, M., Ganjali, M.R., Norouzi, P., Doroudi, T.: Saccharide-coated superparamagnetic Fe_3O_4 nanoparticles (SPIONs) for biomedical applications: an efficient and scalable route for preparation and in situ surface coating through cathodic electrochemical deposition (CED). Mater. Lett. **189**, 290–294 (2017)

15. Karimzadeh, I., Aghazadeh, M., Ganjali, M.R., Norouzi, P., Shirvani-Arani, S.: A novel method for preparation of bare and poly (vinylpyrrolidone) coated superparamagnetic iron oxide nanoparticles for biomedical applications. Mater. Lett. **179**, 5–8 (2016)

16. Karimzadeh, I., Aghazadeh, M., Ganjali, M.R., Dourudi, T.: Effective preparation, characterization and in situ surface coating of superparamagnetic Fe_3O_4 nanoparticles with polyethyleneimine through cathodic electrochemical deposition (CED) method for biomedical applications. Curr. Nanosci. **13**, 167–174 (2017)

17. Karimzadeh, I., Aghazadeh, M., Dourudi, T., Ganjali, M.R., Gharailou, D.: Amino acid coated superparamagnetic iron oxide nanoparticles for biomedical applications through a novel efficient preparation method. J. Clust. Sci. **28**, 1259–1271 (2017)

18. Aslibeiki, B., Kameli, P., Ehsani, M.H., Salamati, H., Muscas, G., Agostinelli, E., Foglietti, V., Casciardi, S., Peddis, D.: Solvothermal synthesis of $MnFe_2O_4$ nanoparticles: the role of polymer coating on morphology and magnetic properties. J. Magn. Magn. Mater. **399**, 236–244 (2016)

19. Kumar, L., Kar, M.: Influence of al^{3+} ion concentration on the crystal structure and magnetic anisotropy of nano crystallines pinel cobalt ferrite. J. Magn. Magn. Mater. **323**, 2042–2048 (2011)

20. Chinnasamy, C.N., Narayanasamy, A., Ponpandian, N., Justin Joseyphus, R., Jeyadevan, B., Tohji, K., Chattopadhyay, K.: Grain size effect on the Néel temperature and magnetic properties of nanocrystalline $NiFe_2O_4$ spinel. J. Magn. Magn. Mater. **238**(2), 281–287 (2002)

21. Chinnasamy, C.N., Narayanasamy, A., Ponpandian, N., Chattopadhyay, K., Shinoda, K., Jeyadevan, B., Tohji, K., Nakatsuka, K., Furubayashi, T., Nakatani, I.: Mixed spinel structure in nanocrystalline $NiFe_2O_4$. Phys. Rev. B **63**(18), 184108–184114 (2001)

22. Lavorato, G.C., Lima, E., Tobia, D., Fiorani, D., Troiani, H.E., Zysler, R.D., Winkler, E.L.: Size effects in bimagnetic CoO/Co Fe2O4 core/shell nanoparticles. Nanotechnology **25**, 355704–355712 (2014)

23. Desautels, R.D., Skoropata, E., Chen, Y.Y., Ouyang, H., Freeland, J.W., Lierop, J.V.: Increased surface spin stability in γ-Fe2O3 nanoparticles with a Cu shell. J. Phys. Condens. Matter **24**, 146001–146011 (2012)

24. Aslibeiki, B., Kameli, P., Manouchehri, I., Salamati, H.: Strongly interacting super spins in Fe_3O_4 nanoparticles. Curr. Appl. Phys. **12**, 812–816 (2012)

25. Mukadam, M.D., Yusuf, S.M., Sharma, P., Kulshreshtha, S.K., Dey, G.K.: Dynamics of spin clusters in amorphous Fe2O3. Phys. Rev. B **72**, 174408–174415 (2005)

26. Millan, A., Urtizberea, A., Silva, N., Palacio, F., Amaral, V., Snoeck, E., Serin, V.: Surface effects in maghemite nanoparticles. J. Magn. Magn. Mater. **312**, 5–9 (2007)

27. Chen, J., Sorensen, C., Klabunde, K., Hadjipanayis, G., Devlin, E., Kostikas, A.: Size-dependent magnetic properties of MnFe2O4 fine particles synthesized by co-precipitation. Phys. Rev. **54**, 9288–9296 (1996)

28. Dodson, H.M., McClelland-Brown, E.: Magnetic blocing temperatures of single-domain grains during slow cooling. J Geophys. Res. **85**, 2625–2637 (1980)

29. Goya, G.F., Morales, M.P.: Field dependence of blocking temperature in magnetite nanoparticles. J Metastable Nanocrystalline Mater. **20**, 673–678 (2004)

30. Hansen, M.F., Mørup, S.: Estimation of blocking temperatures from ZFC/FC curves. J. Magn. Magn. Mater. **203**, 214–216 (1999)

31. Parker, D., Ladieu, F., Vincent, E., Mériguet, G., Dubois, E., Dupuis, V., Perzynski, R.: Experimental investigation of superspin glass dynamics. Appl. Phys. **97**, 10A502–10A505 (2005)

32. Suzuki, Y., Hwang, H.Y., Cheong, S.W., Siegrist, T., Van Dover, R.B., Asamitsu, A., Tokura, Y.: Magnetic anisotropy of doped manganite thin films and crystals. J. Appl. Phys. **83**, 7064–7065 (1998)

33. Rostamnejadi, A., Salamati, H., Kameli, P.: Magnetic properties of interacting La0.67Sr0.33MnO3 nanoparticles. J. Supercond. Nov. Magn. **25**, 1123–1132 (2012)

34. Mydosh, J.A.: Spin Glasses: an Experimental Introduction. Taylor and Francis, London (1993)

35. Bedanta, S., Kleemann, W.: Supermagnetism. J. Phys. D: Appl. Phys. **42**, 013001–013029 (2009)

36. Brown, W.F.: Thermal fluctuations of a single-domain particle. Phys. Rev. **130**, 1677–1686 (1963)

37. Goya, G.F., Berquo, T.S., Fonseca, F.C., Morales, M.P.: Static and dynamic magnetic properties of spherical magnetite nanoparticles. J. Appl. Phys. **94**, 3520–3528 (2003)

38. Masunaga, S.H., Jardim, R.F., Fichtner, P.F.P.: Role of dipolar interactions in a system of Ni nanoparticles studied by magnetic-susceptibility measurements. J. Rivas Phys. Rev. B **80**, 184428–184435 (2009)

39. Rault, J.: Origin of the Vogel–Fulcher–Tammann law in glass-forming materials: the $--$ bifurcation. J. Non-Crystalline Solids **271**, 177–217 (2000)

40. Kura, H., Takahashi, M., Ogawa, T.: Extreme enhancement of blocking temperature by strong magnetic dipoles interaction of α-Fe nanoparticle-based high-density agglomerate. J. Phys. D: Appl. Phys. **44**, 022002–022006 (2011)

41. Alonso, J., Fdez-Gubieda, M.L., Barandiaran, J.M., Svalov, A., Barquin, L.F., Venero, D.A., Orue, I.: Crossover from superspin glass to superferromagnet in FexAg100-x nanostructured thin films (20x50). Phys. Rev. B **82**, 054406–054414 (2010)

42. Dormann, J.L., Bessais, L., Fiorani, D.: A dynamic study of small interacting particles: superparamagnetic model and spin-glass laws. J. Phys. C **21**, 2015–2034 (1988)

43. Dormann, J.L., Fiorani, D., Tronc, E.: On the models for interparticle interactions in nanoparticle assemblies: comparison with experimental results. J. Magn. Magn. Mater. **202**, 251–267 (1999)

44. Dormann, J.L., Fiorani, D., Tronc, E.: Magnetic relaxation in fine-particle systems. Adv. Chem. Phys. **98**, 283 (1997)

45. Mydosh, J.A.: Spin Glasses: an Experimental Introduction. Taylor and Francis, London (1993)

46. Ogielski, A.T., Morgenstern, I.: Critical behavior of three-dimensional Ising spin-glass model. Phys. Rev. Lett. **54**, 928–931 (1985)

47. Fischer, K.H., Hertz, J.: Spin Glasses. Cambridge University Press, Cambridge (1993)

48. Rosensweig, R.E.: Heating magnetic fluid with alternating magnetic field. J. Magn. Magn. Mater. **252**, 370–374 (2002)